Using the radium quartet (^{228}Ra, ^{226}Ra, ^{224}Ra, and ^{223}Ra) to estimate water mixing and radium inputs in Loch Etive, Scotland

Yu-Te Hsieh,[a,1,*] Walter Geibert,[b,c] Pieter van-Beek,[d] Henrik Stahl,[c] Dmitry Aleynik,[c] and Gideon M. Henderson [a]

[a] Department of Earth Sciences, University of Oxford, South Parks Road, Oxford, United Kingdom
[b] School of Geosciences, University of Edinburgh, The King's Buildings, West Mains Road, Edinburgh, United Kingdom
[c] Scottish Association for Marine Sciences (SAMS), Scottish Marine Institute, Oban, Argyll, United Kingdom
[d] Laboratorie d'Etudes en Geophysique et Oceanographie Spatiales (LEGOS), Observatoire Midi- Pyrénées, Toulouse, France

Abstract

The radium (Ra) quartet (^{228}Ra, ^{226}Ra, ^{224}Ra, and ^{223}Ra) has been investigated in Loch Etive, a Scottish fjord, to provide new constraints on water mixing rates and on the inputs of Ra from sediments. Maximum water transport rates for the inflowing estuarine layer at 5 m depth, determined from the excess ^{223}Ra (^{223}Ra$_{ex}$), indicate that this water travels at no more than 2.4 ± 0.2 cm s^{-1} net and that it takes 17 ± 2 d for waters to travel from the mouth to the head of the loch if no horizontal mixing is taken into account. Alternatively, neglecting advection, the short-lived Ra distribution could be explained by horizontal mixing rates of 6.1×10^6 cm^2 s^{-1} (^{223}Ra$_{ex}$) or 9.1×10^6 cm^2 s^{-1} (^{224}Ra$_{ex}$). Periodic overturning circulation plays an important role in resetting chemical cycles in the isolated deep basin of the inner loch. Sediment in this deep basin provides the major input of ^{228}Ra to the isolated deep water, and the accumulation of ^{228}Ra in deep waters allows an assessment of sedimentary fluxes of ^{228}Ra, a poorly constrained aspect of the ^{228}Ra input to the global ocean. The calculated sedimentary ^{228}Ra flux of 2.1 ± 0.2 ($\times 10^9$) atoms m^{-2} yr^{-1} in the inner deep basin is comparable with previous measurements of sedimentary ^{228}Ra inputs from shelf sediments, supporting existing global ^{228}Ra budgets, which are used to assess global rates of groundwater discharge to the ocean.

Estuaries play an important role in the transformation of river water to seawater, showing strong physical and chemical gradients. Estuarine environments provide inputs of trace elements and nutrients to the ocean and can act as a significant filter between the land and the open ocean (Howe et al. 2010). Understanding the physical mixing and advection of waters in these environments is an important aspect of understanding the chemical cycles of estuaries and their role in controlling chemical fluxes to the open ocean.

Since fish farming started in the 1970s, fjords have been increasingly used for aquaculture. The fish farm industry has been found to have negative effects on the fjord ecosystem, such as the spreading of infectious diseases, waste pollution, and marine eutrophication (Cloern 2001). Studies (Karakassis et al. 2000; Skogen et al. 2009) have focused on assessing and modeling the environmental effects of fish farming in fjords. However, the fjord environment is a complex system in terms of water circulation and chemical exchange (Howe et al. 2010). Thus, understanding the physical and chemical environment in fjords would improve the assessment of the environmental effects of fish farming in fjords, which also has a societal and economic value.

Fjords often have glacially over-deepened and semi-enclosed marine basins that provide a particular style of estuarine environment and generate distinct water circulation to control chemical and physical transitions from terrestrial to marine environments (Howe et al. 2010). Fjord circulation systems have also been shown to influence global ocean circulation by regulating glacial runoff and the water exchange between estuarine and coastal environments (Straneo et al. 2011). Despite the interest they generate, water mixing rates and chemical fluxes are not well quantified in typical fjord systems.

Radium (Ra) has four naturally occurring isotopes (^{226}Ra, $T_{1/2} = 1600$ yr; ^{228}Ra, $T_{1/2} = 5.75$ yr; ^{223}Ra, $T_{1/2} = 11.4$ d; and ^{224}Ra, $T_{1/2} = 3.66$ d), the so-called radium quartet (Rama and Moore 1996). These isotopes have been used as powerful tracers for estimation of chemical fluxes to the ocean, including riverine inputs (Li and Chan 1979); sediment inputs (Hancock et al. 2000); and submarine groundwater discharge (SGD) (Charette et al. 2001; Moore et al. 2008). Ra isotopes are produced by the radioactive decay of thorium isotopes, typically in sediments. They are dissolved in pore water and released from sediments into seawater. Ra is therefore a useful tracer for studying chemical interaction at the sediment–water interface. In addition, Ra behaves conservatively (except in the case of its known radioactive decay) once released into seawater. Ra isotopes have therefore also been widely applied to the study of a variety of oceanographic processes and chemical fluxes to the ocean, such as diffusion (Kadko et al. 1987), large-scale ocean mixing (Kaufman et al. 1973; Chung

---

* Corresponding author: yuteh@mit.edu

[1] Present address: Department of Earth, Atmospheric and Planetary Sciences, Massachusetts Institute of Technology, Cambridge, Massachusetts
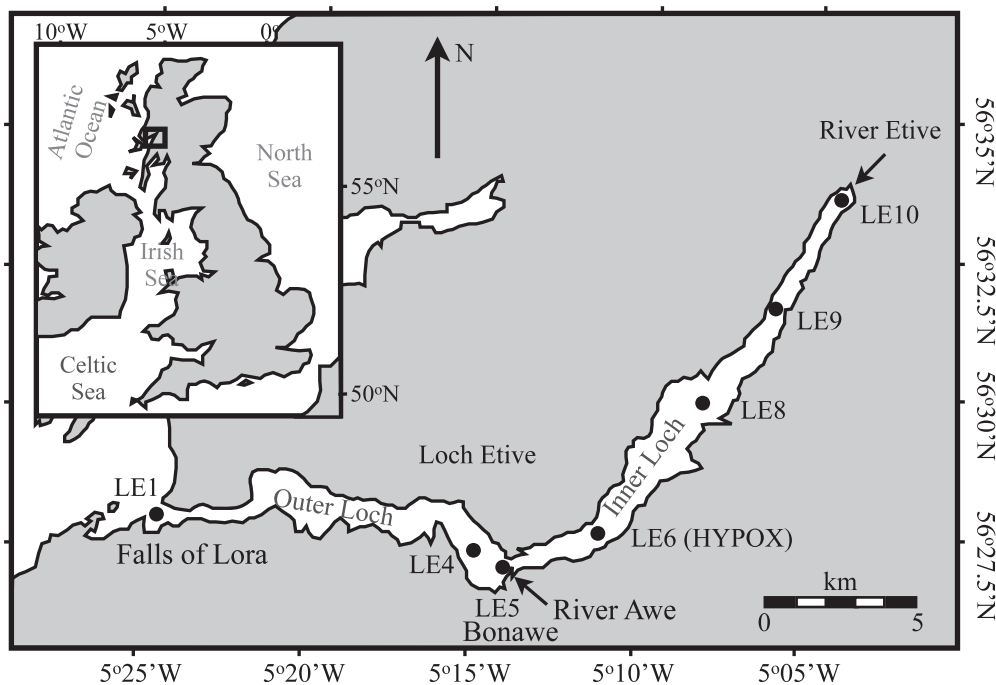
Fig. 1.   Map of Loch Etive with location of sampling sites. The loch is divided into an inner loch and an outer loch by Bonawe Sill at LE5. LE6 is also the HYPOX station in the inner loch for the time-series oxygen data shown in Fig. 3. River Etive and River Awe provide freshwater input into the loch, as indicated by arrows.

1980; Ku and Luo 1994), horizontal and vertical eddy mixing (Broecker et al. 1967; Sarmiento et al. 1976; Van Beek et al. 2008), shelf-water and coastal ocean mixing (Rutgers van der Loeff et al. 1995; Moore 1998, 2000*a*), water-mass and particulate residence time (Broecker et al. 1973), pore-water exchanges (Cochran and Krishnaswami 1980; Webster et al. 1994), and sediment benthic fluxes (Bollinger and Moore 1984; Hammond et al. 1990; Hancock et al. 2000).

An example of the power of Ra isotopes in seawater is their use in assessing global SGD fluxes to the oceans. The inventory of ^{228}Ra in the surface Atlantic Ocean constrains the total SGD input to the ocean (Moore et al. 2008), provided that other important fluxes from rivers and sediments are known. This approach has demonstrated that SGD provides significant input of nutrients and other dissolved species to the ocean, potentially higher than that associated with riverine discharge. Confirming the use of open-ocean ^{228}Ra to assess SGD fluxes requires firm knowledge of the flux of ^{228}Ra from its other major source—marine sediments. Fjords with periodically isolated deep water in contact with marine sediment, such as Loch Etive, provide natural ocean laboratories in which to assess this sedimentary ^{228}Ra flux.

In this study we have provided new constraints on the Ra cycle in the fjord system with a set of analyses on Loch Etive, a Scottish fjord. Resulting surface-water data constrain the rates of mixing in the loch. In the deep waters, the data constrain the sedimentary fluxes of ^{228}Ra, with relevance to assessment of global budgets and SGD fluxes.

Methods

Study area—Loch Etive is a sea loch located on the west coast of Scotland (Edwards and Sharples 1986) (Fig. 1). The loch hosts a number of mussel farms and is used for occasional recreational boating. Details of the bathymetry and sedimentology of the loch have been investigated in a high-resolution seismic and gravity-coring survey (Howe et al. 2001, 2002). The loch is separated into an inner (inland; 145 m maximum depth) and an outer (seaward; 70 m maximum depth) basin by a sill of 13 m depth at Bonawe (*see* Fig. 1). The outer basin is separated from the coastal ocean by another sill, the Falls of Lora. The geological setting is a mixture of igneous and metamorphic rocks, mostly granite, which restricts groundwater penetration through this area. Tide flow drives seawater in and out of the loch. Seawater is mixed with freshwater from River Awe and River Etive from large catchment areas totaling 1400 km^2 (Wood et al. 1973). The mean freshwater discharge is 3038 $\times$ 10^6 m^3 yr^{-1} (Edwards and Sharples 1986).

The hydrology and circulation of Loch Etive are reasonably well known (Edwards and Edelsten 1977) (Fig. 2a). In the inner basin, water masses are structured in three different vertical units (Edwards and Grantham 1986). The freshest waters are observed in a very shallow lens at the surface, with a vertical extent of only tens of centimeters. This layer is dominated by estuarine outflow. Below this surface layer seawater is mixed with smaller amounts of freshwater to varying degrees. While tidal flows lead to reversing flow patterns, in this second layer,
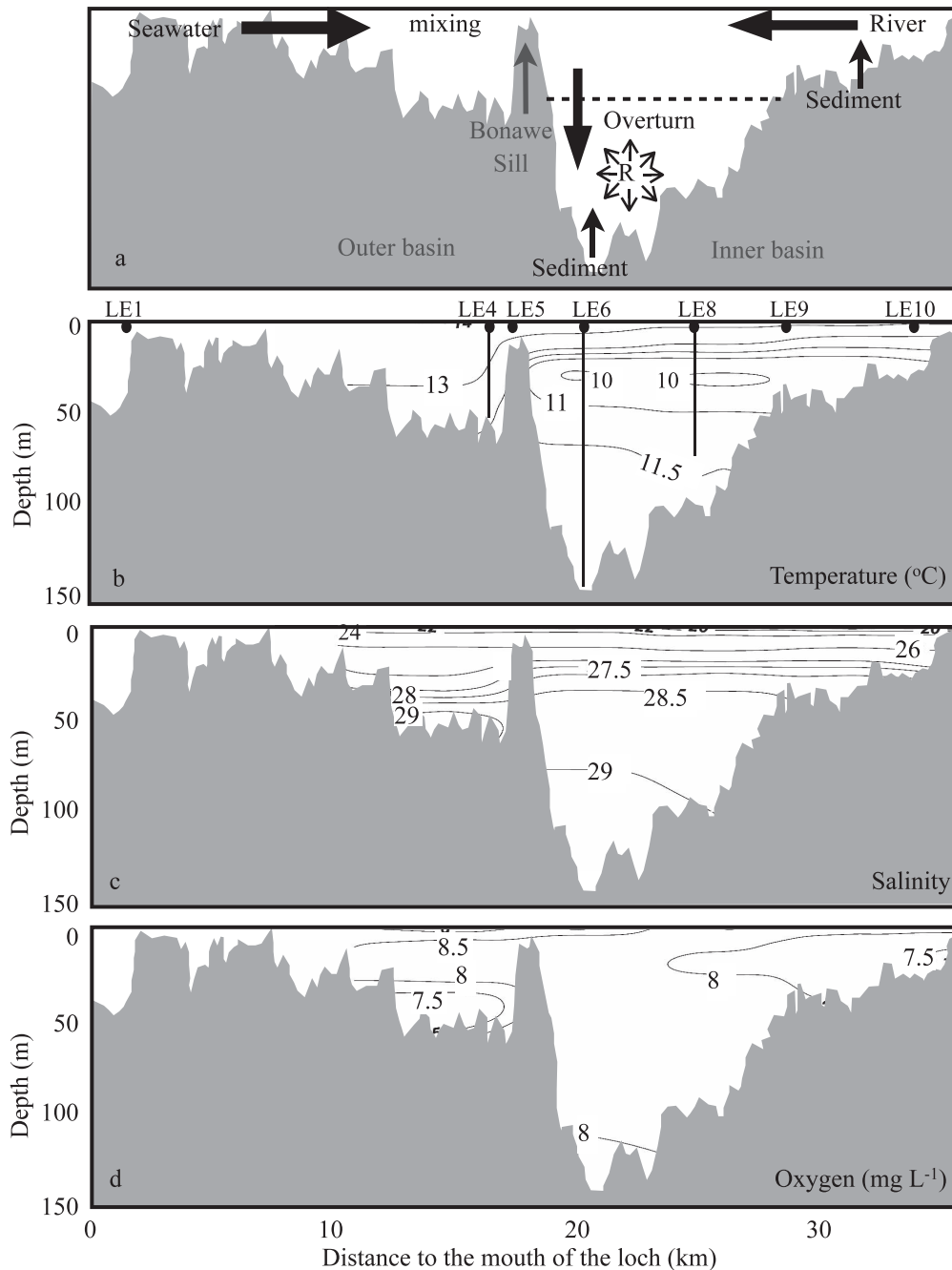
Fig. 2.   (a) Schematic of hydrography and Ra cycles in Loch Etive. The dashed line indicates the inner loch water stratification between mixed surface layer and isolated deep water. In the surface layer, two horizontal arrows indicate water mixing from seawater and river inputs. The arrow across the dashed line presents the inner loch overturning circulation, which happens periodically. Two upward arrows indicate sedimentary Ra input. R is the radioactive decay of Ra. CTD data of (b) temperature (°C), (c) salinity, and (d) oxygen (mg L^{-1}) in Loch Etive on 03 and 04 August 2010. The locations of station are shown by black dots. Samples were collected from the surface at all stations [black dots in (b)] and from three depth profiles at LE4 (54 m), LE6 (136 m), and LE8 (70 m), respectively [solid lines in (b)].

estuarine inflow dominates. This intermediate layer with reduced salinity prohibits flow of waters to depth in the inner deep basin, resulting in a usually stagnant deep third water mass in the inner basin below the depth of a second pycnocline (around 25 m). After a particularly dry period or when temperatures are cold during winter mixing with

freshwater is reduced, and high-salinity dense seawater can flow over the Bonawe Sill (13 m) and sink into the deep inner basin to cause an overturn circulation. The average repeat period for overturn circulation is about 16 months (Edwards and Edelsten 1977), but there is no regular cycle to this overturning period.

Dissolved oxygen is constantly consumed in the deep waters and therefore decreases, so that the level of oxygen in deep waters can be used as an index to monitor overturning events. For example, dissolved oxygen suddenly increased from 0.9 to 9.5 mg L^{-1} during an overturn event in May 2000 and then gradually decreased with time to semi-anoxic levels in the deep inner basin (Austin and Inall 2002). The change of dissolved oxygen also significantly controls other aspects of the chemistry of the loch, such as the manganese (Mn) cycle (Overnell et al. 2002; Statham et al. 2005).

The distribution of Ra isotopes in Loch Etive is dominated by seawater, river, and sediment inputs (Fig. 2a). The concentration of Ra isotopes in the isolated deep water of the inner basin is reset by overturn events. Between such overturns, ^{228}Ra, ^{224}Ra, and ^{223}Ra concentrations can decrease as a result of radioactive decay or increase as a result of addition from the sediment. Measurement of changing Ra concentrations in the deep waters therefore has potential to be used to assess the rates of sedimentary Ra input to seawater.

Sampling methods—Water samples were collected aboard the R. V. *Calanus* during a 2-d cruise on 03 and 04 August 2010 in Loch Etive. Samples from 5 m depth were collected from seven stations from the mouth of the loch (LE1), the outer loch (LE4 and LE5), the inner loch (LE6, LE8, and LE9), and the head of the loch (LE10) (Fig. 1). Deep-water samples were collected from three stations at LE4, LE6, and LE8 (Fig. 2b). Sta. LE6 was reoccupied 10 months later on 08 June 2011 to assess the temporal evolution of Ra in the deep loch.

Each sample consisted of water from twelve 5 liter Niskin bottles mounted on a conductivity–temperature–depth (CTD) rosette and fired at the same depth as one another. Resulting 60 liter samples were stored briefly in cubitainers before shipboard pre-concentration of Ra. Samples were passed through a column of MnO_2-coated acrylic fiber by gravity at a flow rate < 0.5 L min^{-1} to concentrate the Ra (Moore et al. 1985). For a summary of methods and considerations of Ra sampling refer to Moore (2008). After sampling, Mn fibers were rinsed three times with Milli-Q water to remove adhering salt and squeezed to reduce liquid content. A subsample of 250 mL was also collected from each location and depth for a separate measurement of ^{226}Ra concentration (Foster et al. 2004).

Measurements—Seawater ^{224}Ra and ^{223}Ra by Ra delayed-coincidence counting system (RaDeCC): Mn -fiber samples were first counted using a four-channel RaDeCC for ^{224}Ra and ^{223}Ra activities (Moore and Arnold 1996). Fibers were then stored for 2–3 weeks before a second count on the same device to determine how much of the ^{224}Ra was supported by thorium-228 (^{228}Th). When required, as a result of still-elevated activities in the second count, a third and final count was performed to assess how much of the ^{223}Ra was supported by actinium-227 (^{227}Ac) (Geibert et al. 2008). Supported ^{223}Ra and ^{224}Ra activities, as measured on the second and third counts, were subtracted to give the excesses of ^{223}Ra and ^{224}Ra (^{223}Ra$_{ex}$

and ^{224}Ra$_{ex}$, respectively) in each sample. The RaDeCC was calibrated regularly with two standard samples from the parent nuclides of short-lived Ra, ^{227}Ac, and ^{232}Th, which had been obtained from the International Atomic Energy Agency–Marine Environmental Laboratories, Monaco, in 2009 (Scholten et al. 2010). As a result of the relatively low activities of short-lived Ra for a coastal environment, the overall uncertainties of ^{224}Ra and ^{223}Ra are 10% to 40% (2 standard errors [SE]).

Seawater ^{228}Ra and ^{226}Ra by multi-collector inductively coupled plasma mass spectrometry (MC-ICP-MS)—The long-lived Ra isotopes (^{226}Ra and ^{228}Ra) were measured using a newly developed technique, which makes use of MC-ICP-MS (Hsieh and Henderson 2011). After RaDeCC counting, Mn fibers were ashed in a furnace and then leached with HCl for the purification of Ra. Ra was precipitated by $Sr(Ra)SO_4$ in the leaching solution and then converted to $Sr(Ra)CO_3$ for dissolution (Cohen and O'Nions 1991) before ion-exchange column chemistry (AG50-X8 and Sr-spec). The non-spiked Mn fiber samples were measured for the ^{228}Ra : ^{226}Ra activity ratios. The ratios were then multiplied by ^{226}Ra concentrations to calculate ^{228}Ra concentrations. For measurement of ^{226}Ra concentrations, water samples (250 mL) were spiked with an enriched ^{228}Ra spike following the procedure described in Foster et al. (2004). In short, Ra is precipitated with $CaCO_3$ in seawater and then purified by ion exchange columns (AG1-X8, AG50-X8, and Sr-Spec) before analysis. The pure Ra aliquot was analyzed by MC-ICP-MS, with ^{228}Ra and ^{226}Ra simultaneously measured in two ion counters. Bracketing measurements of a uranium standard, Certified Reference Material–145, were used to assess and correct for mass bias and ion-counter gain between each sample. Chemical blanks were monitored for the whole procedure and are less than 1% of ^{226}Ra of the sample and not detectable for ^{228}Ra. The machine memory was also monitored and corrected between each measurement. The overall uncertainties of ^{226}Ra and ^{228}Ra are 3% to 4% (2 SE). The improved analytical precision allows us to more precisely calculate water mixing and Ra fluxes in Loch Etive.

Results

Temperature, salinity, and oxygen data—Temperature, salinity, and oxygen data are presented in Fig. 2. While salinity in the surface layer varies between 2 and 18 with a high dissolved oxygen of ~ 9.5 mg L^{-1} and temperatures around 15°C, samples at 5 m all have salinities of > 24 (Fig. 3a). At depth, the inner loch had a homogeneous water mass below 30 m, with temperatures of 11–12°C, salinity of 28–29, and dissolved oxygen of 7.5–8.5 mg L^{-1} during the August 2010 cruise (Fig. 4f). A colder water layer with temperature < 10°C and lower dissolved oxygen of ~ 8 mg L^{-1} covered the whole inner loch between 20 and 30 m. In the outer loch, deep water showed oxygen depletion (~ 7 mg L^{-1}) below 42 m.

Time-series oxygen data (Fig. 5) have been collected for the Hypox mooring (Stahl 2011) from December 2009 to January 2012 at 124 m at the inner-loch deep-basin
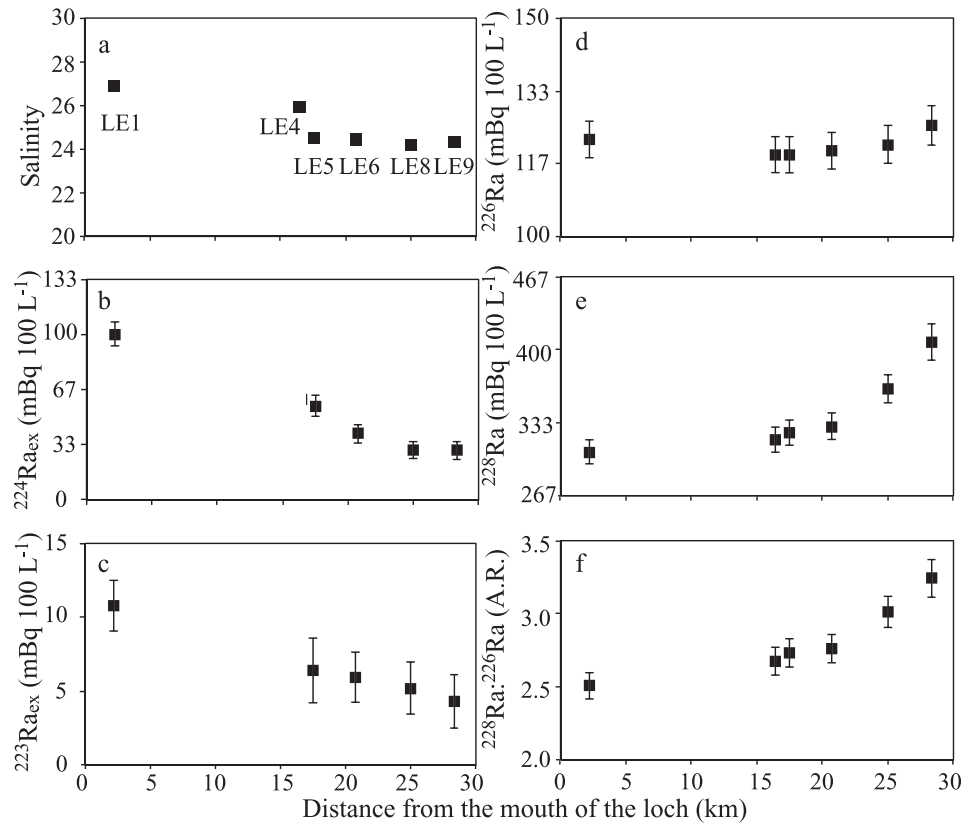
Fig. 3.   Surface profiles of (a) salinity, (b) $^{224}Ra_{ex}$, (c) $^{223}Ra_{ex}$, (d) ^{226}Ra, (e) ^{228}Ra (mBq 100 L^{-1}), and (f) $^{228}Ra : ^{226}Ra$ activity ratio at 5 m (except LE4 at 10 m) in Loch Etive plotted with the distance from the mouth of the loch. Note the relatively slight change in salinity within the loch, relative to the larger and generally systematic changes of Ra concentration with distance from the mouth of the loch.

observatory (LE6 in Fig. 1). The Hypox time-series oxygen data generally show consistent results with the CTD measurements. The data indicate that deep water in the inner loch had just overturned between 22 and 28 June 2010, before our sampling. Oxygen concentrations in the deep inner loch decrease from 11 mg L^{-1} to 3 mg L^{-1} with time after this overturn circulation. Between the first and the second cruises (August 2010–June 2011), time-series oxygen data indicate that the deep water of the inner basin had remained isolated since the overturn event in late June 2010.

Ra isotopes—The radioactivity of Ra isotopes is presented in millibequerel (mBq) in this article. To convert from mBq to disintegration per minute (dpm), the unit commonly used in the marine radioactive research community, 1 mBq is equal to 0.06 dpm.

Concentrations of $^{223}Ra_{ex}$ and $^{224}Ra_{ex}$ range from below the detection limit (< 1.7 mBq 100 L^{-1}) to 33 mBq 100 L^{-1} and 203 mBq 100 L^{-1}, respectively (Table 1). In the water column of the inner basin (Fig. 4d,e), $^{223}Ra_{ex}$ and $^{224}Ra_{ex}$ show higher activities in the subsurface layer at the 5 m depth (6 and 40 mBq 100 L^{-1}, respectively), no measureable activity at mid-depths, and then an increase toward the basin floor (3.0 and 37 mBq 100 L^{-1}, respectively). However, $^{223}Ra_{ex}$ and $^{224}Ra_{ex}$ from the second cruise at LE6 are both below the detection limit in deep-water samples at all depths

in the inner basin. At 5 m depth (Fig. 3b,c), $^{223}Ra_{ex}$ and $^{224}Ra_{ex}$ are both found to decrease with distance away from the mouth of the loch (from 10.8 to 4.3 mBq 100 L^{-1} and from 100 to 30 mBq 100 L^{-1}, respectively).

The activities of ^{226}Ra and ^{228}Ra in the water samples range from 72 to 143 mBq 100 L^{-1} and from 295 to 407 mBq 100 L^{-1}, respectively. The activity ratios of $^{228}Ra : ^{226}Ra$ show a range from 2.5 to 4.4 (Table 1). In the inner basin (Fig. 4a), ^{226}Ra activity shows a constant distribution (137 ± 7 mBq 100 L^{-1}) below 30 m during the first and second cruises. ^{228}Ra activity is also constant with depth (363 ± 23 mBq 100 L^{-1}) in the first cruise but significantly decreases, from 377 to 137 mBq 100 L^{-1}, at 90 m during the second cruise (Fig. 4b). In the outer basin, the water column shows a layer of oxygen depletion below 42 m, with constant salinity and temperature. In this layer, ^{226}Ra and ^{228}Ra both show the highest values of 138 and 392 mBq 100 L^{-1}, respectively, in the water column. At 5 m depth, ^{226}Ra activities are relatively constant between 118 and 125 mBq 100 L^{-1} (Fig. 3d), but ^{228}Ra activities increase from 307 to 407 mBq 100 L^{-1} (Fig. 3e) toward the head of the loch.

Discussion

Surface-water mixing in Loch Etive—The short-lived Ra isotopes, ^{223}Ra and ^{224}Ra, reflect horizontal mixing and net

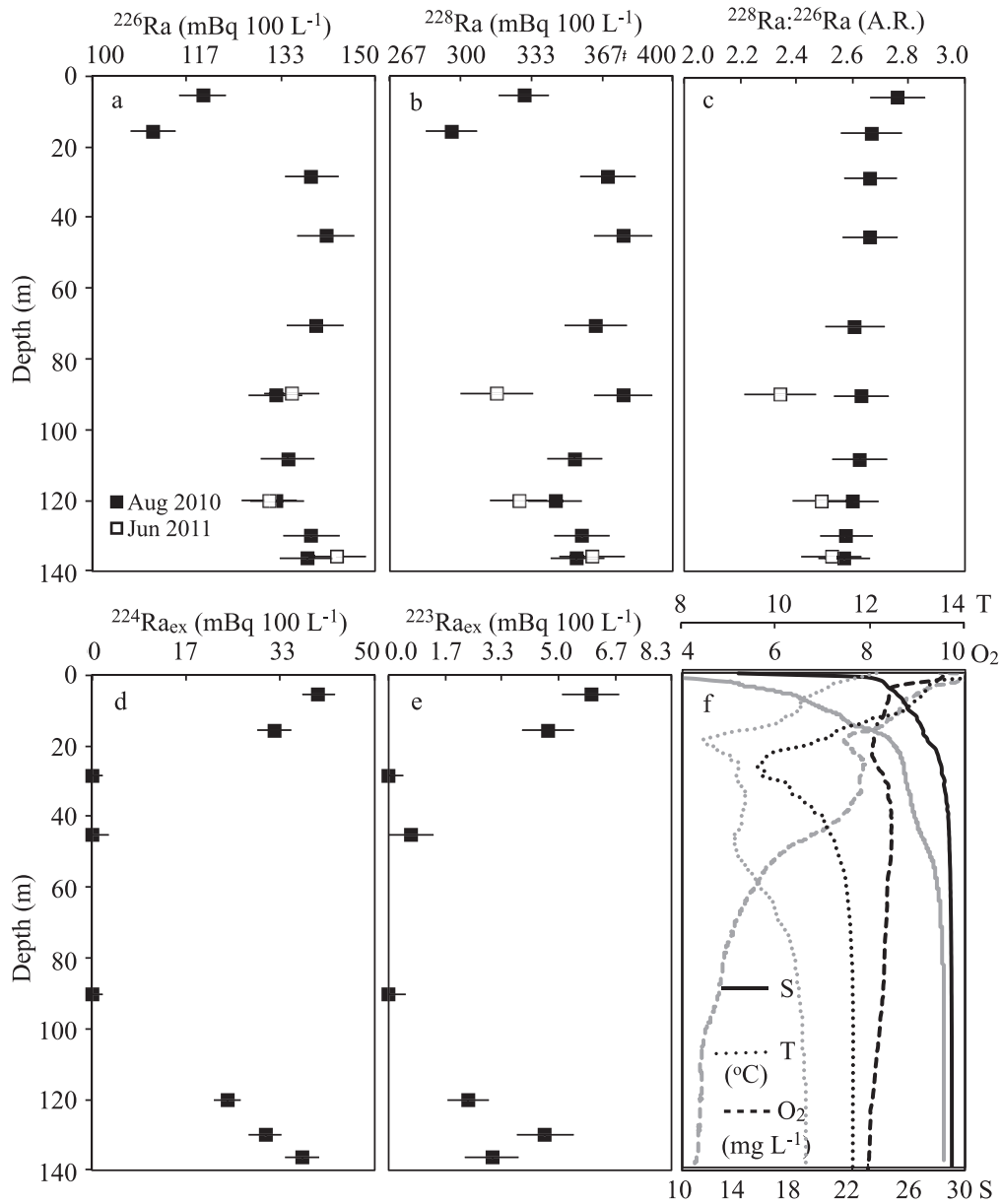Fig. 4. Water-column profiles of (a) ^{226}Ra, (b) ^{228}Ra, (c) ^{228}Ra : ^{226}Ra, (d) ^{224}Ra$_{ex}$, (e) ^{223}Ra$_{ex}$ (mBq 100 L^{-1}), and (f) salinity, temperature, and oxygen in the inner basin of Loch Etive. Data are from Sta. LE6, with the black line and filled squares representing data from 03 August 2010 and the gray line and open squares representing data from 08 June 2011. A. R. indicates activity ratio.

advective transport. Key to their application here is the consideration of the specific hydrographic features of Loch Etive. The typical features of an estuary, the outward transport of fresh and brackish water at the surface, and the inward transport of seawater at deeper layers are present in Loch Etive, as seen in the salinity data, but they are forced through two shallow sills. The outer sill, the Falls of Lora, leads to turbulent mixing over the entire depth, and the water produced here has a salinity > 26 (LE1 and LE2). At Bonawe Sill (13 m), which separates the inner and outer basins, the net outward movement of fresher water is more restricted to the very surface, whereas the water at 5 m depth has a near-constant salinity of just above 24. The latter is the water that will mainly enter the

inner basin during high tides. This combination of inflow and outflow at different depths at the same location has previously been described by Edwards and Grantham (1986). As our transect in surface waters is located at 5 m depth, considerably below the brackish surface layer, our data are likely to reflect the net inflowing layer. The salt introduced at 5 m depth will leave the inner basin as part of the brackish surface layer, with a net discharge that is larger than the inflow, as a result of the addition of freshwater from rivers. At 5 m depth, salinity decreases from 26.9 to 24.3 (Fig. 3a) toward the head of the loch. Activities of ^{223}Ra$_{ex}$ and ^{224}Ra$_{ex}$ decrease in concert with this salinity change (Fig. 3b,c). The decrease in activity of ^{223}Ra$_{ex}$ and ^{224}Ra$_{ex}$ with distance (x) can most readily be
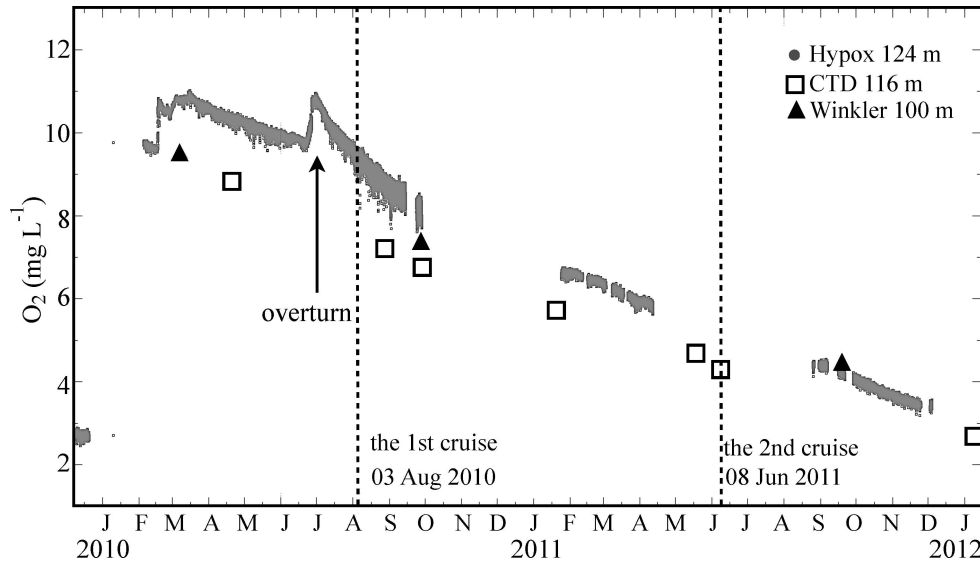
Fig. 5. Time-series oxygen data (HYPOX) at 124 m at the inner-loch deep-basin. The data (gray dots) are collected from December 2009 to January 2012 and are compared with the CTD (open squares) and Winkler (black triangles) data at 116 m and 100 m, respectively.

explained by the radioactive decay of Ra entering the loch in seawater as that water is transported toward the head of the loch by mixing or by advection.

The estuarine circulation in Loch Etive indicates that advective transport dominates Ra budgets and allows calculation of a maximum inflow rate in the estuarine inflow layer at 5 m depth. Alternatively, Ra might be controlled by mixing into the Loch, and we therefore assess a pure mixing scenario that assumes that the tidal in- and outflow are not vertically separated. The horizontal magnitude of salinity change is small at the 5 m depth (Fig. 3a) and is therefore consistent with both scenarios.

In an advection-only scenario, the distribution of $^{223}Ra_{ex}$ and $^{224}Ra_{ex}$ in the subsurface layer at the 5 m depth can be expressed by the following equation:

$$w\partial A/\partial x = \lambda A \qquad (1)$$

where w is the mean water transport rate; x is the distance from the mouth of Loch Etive; A is $^{223}Ra_{ex}$ or $^{224}Ra_{ex}$ activity; and λ is the decay constant for ^{223}Ra (0.0608 d^{-1}) or ^{224}Ra (0.189 d^{-1}).

The solution for w is then given by

$$w = \lambda x/\ln(A_i/A) = X_{1/2}/T_{1/2} \qquad (2)$$

where A_i is the initial activity of $^{223}Ra_{ex}$ and $^{224}Ra_{ex}$ (i.e., at LE1); $X_{1/2}$ is the distance at which $A = 0.5A_i$; and $T_{1/2}$ is the half-life of ^{223}Ra or ^{224}Ra. Based on the data in Fig. 3b and c, we obtain water transport rates of 6.1 and 2.4 cm s^{-1} from $^{224}Ra_{ex}$ and $^{223}Ra_{ex}$, respectively. For comparison, previous measurements made by current meters show that the water transport rates are usually below their detection limit of 5 cm s^{-1} in the water 40 m below the surface in Loch Etive (Edwards and Edelsten 1977). Inall et al. (2004) found an average speed of 20 cm s^{-1} using a current meter around the Bonawe Sill during spring tides. In terms of

depth, distance, and timescale, the Ra-derived water transport rates appear to reflect a long-term (days to weeks) average water transport throughout the surface layer, which is more suitable for assessing long-term average chemical fluxes but not for short-term (minutes to hours) variability.

The water transport rate calculated by $^{224}Ra_{ex}$ is ≈ 2.5 times higher than the rate calculated by $^{223}Ra_{ex}$. Assuming that seawater inflow is the only input for $^{223}Ra_{ex}$ and $^{224}Ra_{ex}$ to the surface water, $^{223}Ra_{ex}$ should show less decay with distance than does $^{224}Ra_{ex}$ as a result of its longer half-life. Put another way, if the $^{223}Ra_{ex}$-derived mixing is correct, observed $^{224}Ra_{ex}$ values should decrease rapidly in the loch to values significantly lower than were observed. This discrepancy can be explained if there is an additional input of $^{224}Ra_{ex}$ to the surface water (*see* discussion below). The slower transport rate, derived from $^{223}Ra_{ex}$, is more likely to be a true estimate of transport and indicates a rate of 2.4 $\pm$ 0.2 cm s^{-1}, which is broadly consistent with a previously estimated horizontal mixing transport rate of $\approx$ 3.5 cm s^{-1} in the inner loch basin (Inall 2009). This results in a seawater transport time of 17 $\pm$ 2 d from the mouth to the head of Loch Etive in the layer at 5 m depth. If there is a source of ^{223}Ra within the loch, in addition to ^{224}Ra, then these transport rates would be lower, but such a source appears unlikely, as discussed below.

In the alternative mixing-only scenario, following the approach in Moore (2000*a*), we obtain a horizontal mixing rate of 6.1 $\times$ 10^6 cm^2 s^{-1} ($^{223}Ra_{ex}$) or 9.1 $\times$ 10^6 cm^2 s^{-1} ($^{224}Ra_{ex}$) in the layer at 5 m depth (*see* Fig. 6). The value from ^{224}Ra is possibly slightly affected by some additional inputs from the Rivers Awe and Etive, as discussed below. The mixing rates represent an upper limit for average horizontal mixing in the period observed, as they neglect the possible net advection in this subsurface layer. The actual situation in Loch Etive will include both advective terms (if

Table 1. Radium isotopic data in Loch Etive.

Sample station	Date	Depth (m)	Salinity	T (°C)	Oxygen (mg L⁻¹)	^{226}Ra (mBq 100 L⁻¹)	^{228}Ra (mBq 100 L⁻¹)	$^{228}Ra:^{226}Ra$ (activity ratio)	$^{223}Ra_{ex}$ (mBq 100 L⁻¹)	$^{224}Ra_{ex}$ (mBq 100 L⁻¹)
LE1	04 Aug 2010	5	26.9	13.8	8.9	122±5	307±12	2.5±0.1	10.8±1.7	100±7
LE4	03 Aug 2010	1	18.1	15.1	10.1	102±3	315±12	3.1±0.1	7.3±2.3	60±8
		10	25.9	13.1	8.4	118±3	318±12	2.7±0.1	0.5±1.5	10±7
		23	26.8	13.5	8.5	127±5	327±12	2.6±0.1	bd	bd
		54	29.2	12.2	7.0	138±5	392±15	2.8±0.1	5.2±2.2	65±8
LE5	03 Aug 2010	5	24.5	13.3	8.5	118±5	325±12	2.7±0.1	6.3±2.2	57±7
LE6	03 Aug 2010	5	24.5	13.2	8.3	120±5	330±12	2.8±0.1	6.0±1.7	40±5
		15	26.3	12.4	8.1	112±3	295±12	2.7±0.1	4.7±1.5	32±7
		28	28.1	9.5	8.4	138±5	370±13	2.7±0.1	bd	bd
		45	28.8	11.0	8.3	142±5	377±13	2.7±0.1	bd	bd
		70	29.0	11.6	8.3	140±5	363±15	2.6±0.1	bd	bd
		90	29.0	11.6	8.2	132±5	377±13	2.6±0.1	bd	bd
		108	29.0	11.6	8.2	135±5	353±13	2.6±0.1	bd	bd
		120	29.0	11.6	8.0	133±5	345±13	2.6±0.1	2.3±1.2	23±5
		130	29.1	11.6	8.0	138±5	357±13	2.6±0.1	4.7±1.5	30±5
		136	29.1	11.6	8.0	138±5	355±13	2.6±0.1	3.0±1.5	37±7
	08 Jun 2011	90	28.5	10.5	4.8	135±5	317±17	2.3±0.1	bd	bd
		120	28.5	10.6	4.4	132±5	327±13	2.5±0.1	bd	bd
		136	28.5	10.6	4.3	143±5	362±15	2.5±0.1	bd	bd
LE8	04 Aug 2010	5	24.2	12.7	7.9	122±5	365±13	3.0±0.1	5.2±1.8	30±5
		33	28.3	9.9	8.2	138±5	365±13	2.7±0.1	bd	bd
		70	28.9	11.4	8.2	138±5	363±15	2.6±0.1	bd	bd
LE9	04 Aug 2010	5	24.3	12.4	7.7	125±5	407±17	3.2±0.1	4.3±1.8	30±5
LE10	04 Aug 2010	1	4.1	14.7	9.8	72±3	313±13	4.4±0.2	33.7±3.0	203±10

All errors are given at ±2 SE. bd, below detection limit; T, temperature.
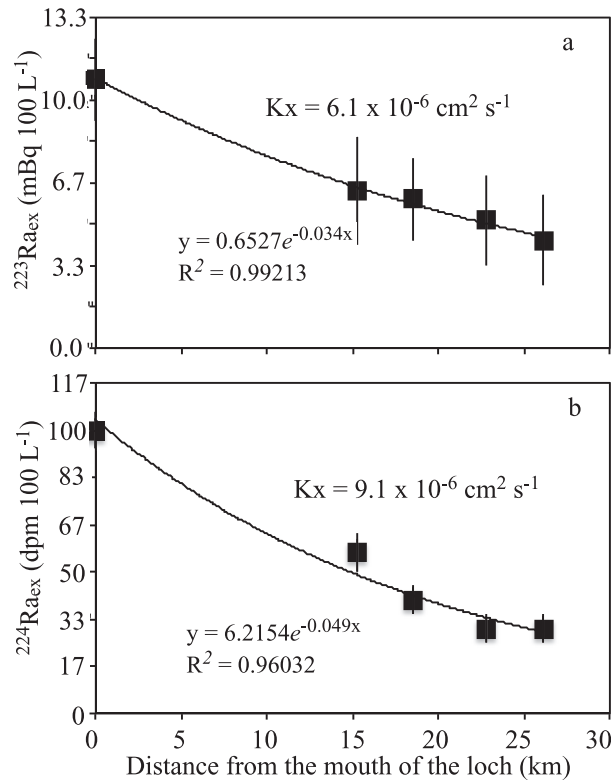
Fig. 6. Profiles of (a) $^{223}Ra_{ex}$ and (b) $^{224}Ra_{ex}$ at 5 m plotted with the exponential regression line (solid line) and the calculated horizontal mixing coefficient (K_x) in the mixing-only scenario.

resolving tidal cycles or when including overturning events) as well as a mixing component (when looking at timescales that integrate tidal fluctuations or during slack tides).

Sedimentary inputs of ^{224}Ra and ^{228}Ra to the surface water—Based on the advection-only scenario discussed above, $^{223}Ra_{ex}$-derived water transport rate (Fig. 7a) and the radioactive decay of ^{224}Ra can be used to calculate a theoretical curve of $^{224}Ra_{ex}$ (solid line) in the surface water with distance from the mouth to the head of loch (Fig. 7b). If there was no additional input of ^{224}Ra to the surface water, the decrease of $^{224}Ra_{ex}$ activity should follow this theoretical curve, but observed activities fall above this expected decay curve.

The source of $^{224}Ra_{ex}$ likely to explain these higher values is the shelves of the loch, particularly around Bonawe, where these shelves are pronounced and where strong cross-sill flow (Inall et al. 2004; Stashchuk et al. 2007) may enhance the release of alpha-recoiled ^{224}Ra from sediments on the sill flat to surface water. $^{224}Ra_{ex}$ concentrations continue to decrease further into the loch beyond the Bonawe Sill, but this decrease cannot be explained by simple exponential decay, and a further source of ^{224}Ra is required at the head of the loch (*see* the gray area highlighted in Fig. 7b). In contrast, the Bonawe Sill does not increase ^{228}Ra to the surface water. This is due to the high flushing rate and the shorter contact time of water and the host rock on the sill flat. To build up high Ra activity in water, ^{228}Ra needs a much longer contact time than does ^{224}Ra (Porcelli and Swarzenski 2003).
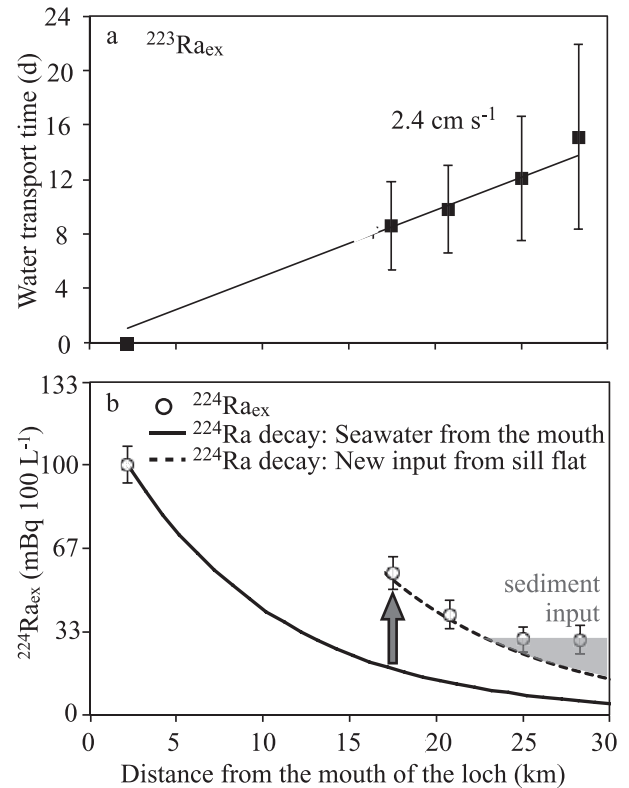

Fig. 7. (a) Surface-water transport time calculated from the radioactive decay of $^{223}Ra_{ex}$ with the distance from the mouth of the loch in the advection-only scenario. (b) Predicted $^{224}Ra_{ex}$ decay curves based on the $^{223}Ra_{ex}$-derived water transport rate (2.4 cm s^{-1}): the solid line represents the expected change in ^{224}Ra if it is provided only from seawater outside the loch. The dashed line demonstrates the need for additional input of ^{224}Ra from the sill flat at LE5 and is curved to represent expected mixing if there is no further source further into the loch. The gray shaded regions indicate additional offset of $^{224}Ra_{ex}$ from the decay curve due to the additional sediment input at the head of the loch.

The additional source of $^{224}Ra_{ex}$ at the head of the loch is associated with higher ^{228}Ra and $^{228}Ra:^{226}Ra$ ratios in surface waters (Fig. 3e,f). The increase of ^{228}Ra seen toward the head of the loch (Fig. 3e) in the surface water is not controlled by radioactive decay, as the half-life of ^{228}Ra is significantly longer than the surface-water transport rate, so an input of ^{228}Ra is required. The decrease in salinity (from 24.5 to 24.3) in the 5 m depth waters at the head of the loch is small (Fig. 3a), indicating that the required inputs of ^{228}Ra and ^{224}Ra to this layer are not from freshwater or groundwater inputs. As at Bonawe in the middle of the loch, shelf sediments in the inner loch are likely to be the source of this ^{228}Ra and ^{224}Ra. The bathymetry of Loch Etive shows a large area of the shelf (with water depths < 15 m) at the head of the loch (Howe et al. 2001) where riverine sediment depositions might be releasing ^{228}Ra and ^{224}Ra to surface water.

Surface-water ^{228}Ra and $^{224}Ra_{ex}$ concentrations at Sta. LE9 minus seawater values can be used to estimate the excess $^{224}Ra:^{228}Ra$ activity ratio from the sediment input. The resulting value is 0.15 ± 0.02, which is lower than the
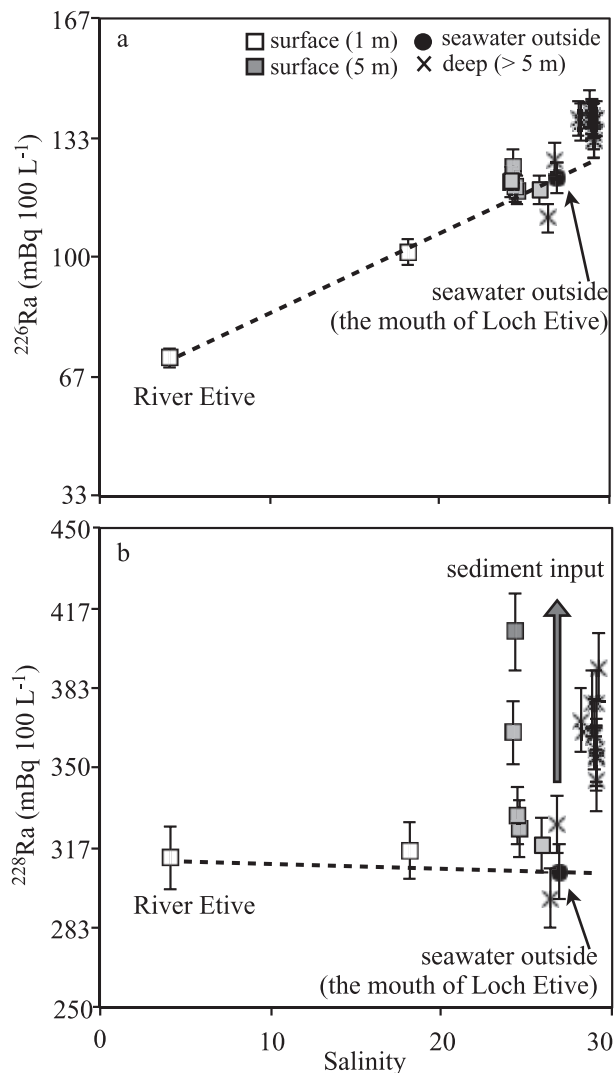
Fig. 8. The activities of ^{226}Ra (a) and ^{228}Ra (b) plotted against salinity in Loch Etive. For these longer-lived Ra isotopes, there is insufficient time for significant changes in activity due to decay in the loch waters. A mixing curve is therefore expected between the waters of River Etive and the seawater outside of the Loch. ^{226}Ra activities fall close to this mixing line, but ^{228}Ra activities show somewhat higher ^{228}Ra values as a result of the addition of ^{228}Ra from sediments to water within the loch.

expected ratio of 1.0 based on the secular equilibrium ^{228}Th : ^{232}Th ratio in sediments. This could be explained by the radiogenic decay of ^{224}Ra since the last time the water was in contact with sediments and the apparent water age (Moore 2000b) in the loch surface layer. Based on the model in Moore (2000b), the apparent age could be calculated by comparing the estimated ^{224}Ra$_{ex}$: ^{228}Ra activity ratio of 0.15 to the expected ratio of 1.0. The estimate age is 10.1 d in the surface water at LE9, which is comparable to the estimated water residence time (17 d) in the surface Loch Etive.

Compared to ^{224}Ra and ^{228}Ra inputs, the input of ^{223}Ra from shelf sediments is insignificant in Loch Etive because the bedrock of this region is granite, which usually has a

lower content of uranium (U) (^{235}U, grandparent of ^{223}Ra) than of Th (^{232}Th, parent and grandparent of ^{228}Ra and ^{224}Ra, respectively). For example, the granite in the Isle of Skye, Scotland, has an average ^{238}U concentration of 1.1 μg g^{-1} and a ^{232}Th concentration of 7.3 μg g^{-1} (Tammemagi 1976). Based on the atomic ratios of ^{232}Th : ^{238}U (6.6) and ^{238}U : ^{235}U (137.88) in granite, the estimated input (or production) of ^{223}Ra activity is about 9100 times smaller than that for ^{224}Ra and ^{228}Ra from the sediment or bedrock of Loch Etive. However, bedrock or shelf sediments may not be able to entirely explain the input of ^{223}Ra outside the mouth of Loch Etive. Outside the Loch, Ra has multiple sources from sediments, seawater, and recirculated seawater.

Riverine inputs, seawater inflow, and shelf sediments in the inner loch are the three major end members for Ra in Loch Etive. Deviations from the mixing line between freshwater and seawater on the plots of ^{226}Ra and ^{228}Ra against salinity (Fig. 8) allow sedimentary inputs to be clearly identified. For ^{226}Ra (Fig. 8a), the trend shows two end members mixing between seawater and river inputs. For ^{228}Ra (Fig. 8b), the mixing between seawater and river inputs is equal. However, the magnitude of these deviations from the two end members mixing between the head and the mouth of the loch indicates that the sediment input could contribute 10–23% of the ^{228}Ra to the surface water.

Ra cycles and overturn circulation in the inner loch basin— Overturning circulation plays an important role in controlling Ra cycles in the isolated deep waters of Loch Etive. In the inner basin, the vertical water profiles of ^{226}Ra and ^{228}Ra show uniform distributions with depth in the water column below 20 m. This can be interpreted as due to the recent overturning of loch waters, known to have occurred, based on O$_2$ data, 1 month prior to our major sampling. This event reset the ^{226}Ra and ^{228}Ra activities in the water column (Fig. 4a,b) and may have led to temporary perturbation of deep-water ^{223}Ra and ^{224}Ra through sediment disturbance or enhanced vertical mixing. Assuming that ^{224}Ra is in steady state, the vertical profile of ^{224}Ra$_{ex}$ activity (Fig. 4d) indicates a strong vertical mixing coefficient (K$_z$) of 18.8 cm^2 s^{-1}, based on the commonly used one-dimensional diffusion model summarized in Ku and Luo (2008). In contrast, a much lower value of K$_z$ of < 2.5 cm^2 s^{-1} is obtained in the well-stratified deep water in the inner loch (Inall 2009), which also explains the observations of low ^{224}Ra$_{ex}$ and ^{223}Ra$_{ex}$ activities (below detection limit) during the second cruise.

The ^{228}Ra activity in inner loch water below 20 m is rather constant between 345 and 377 mBq 100 L^{-1} (Fig. 4b), which is about 10–17% higher than the value of 312 mBq 100 L^{-1} in the ^{228}Ra-salinity mixing relationship between seawater and freshwater in Fig. 8b. This indicates either that the mixing relationship was somewhat different at the time of the last overturn or that the additional input of ^{228}Ra from the loch shelf sediment also contributes ^{228}Ra to the new deep waters during overturn. In this latter situation, surface waters incorporate additional ^{228}Ra from shelf sediments before and as they overturn and fill the deep loch.

Sedimentary ^{228}*Ra flux in the inner loch basin*—Following overturn, the deep water in the inner basin is isolated, and addition of further ^{228}Ra can happen only from sediments below the loch. Addition of groundwater to the deep loch is not expected, given the granite basement, and there is no evidence for such flow from salinity measurements in this or other studies. The activity of ^{228}Ra is therefore controlled only by the balance between radioactive decay and sedimentary inputs.

The sedimentary input flux of ^{228}Ra in the deep basin can be calculated from data for Ra isotopes from the two cruises in August 2010 and June 2011. Oxygen data indicate that deep waters of the inner loch remain isolated between these dates and that there are no overturning events. The ^{226}Ra activity shows very consistent results between the two cruises in the deep inner basin, which supports such isolation (Fig. 4a). Changes in ^{226}Ra are not expected because the half-life is long compared to the period between overturning events, allowing insufficient time for decay and little chance for alpha-recoil from sediments. However, the data for ^{228}Ra activity and ^{228}Ra : ^{226}Ra ratio show a significant decrease at 90 m in the inner basin from August 2010 to June 2011 (Fig. 4b,c). This implies that the ^{228}Ra input from the deep basin sediment is not high enough to balance the output by radioactive decay in the water column.

A simple box model is used to calculate the average ^{228}Ra sediment flux in the inner basin. Because of the somewhat variable distribution of ^{228}Ra activity in the water column (Fig. 4b), the activity ratios of ^{228}Ra : ^{226}Ra in Fig. 9 are used to normalize the ^{228}Ra activities. The activities of ^{226}Ra between these two cruises are relatively constant, with a mean value of 137 ± 3 mBq 100 L^{-1}. At the time of the first cruise, the average activity ratio of ^{228}Ra : ^{226}Ra in the deep water is constant (2.6 ± 0.1) because an overturn event reset the value a month before sampling. Therefore, the normalized ^{228}Ra activity is 355 ± 8 mBq 100 L^{-1}. Assuming no subsequent overturning and that there is no sediment input, the activity of ^{228}Ra should decrease from 355 to 320 mBq 100 L^{-1}, and the activity ratio should decrease from 2.60 to 2.34 as a result of the radioactive decay of ^{228}Ra. At the time of the second cruise, ^{228}Ra activities higher than 320 mBq 100 L^{-1} or activity ratios higher than 2.34 demonstrate input of ^{228}Ra from deep basin sediments.

The total additional ^{228}Ra contributed to deep waters is calculated from the observed increase in ^{228}Ra above that expected from decay. The integrated increase of ^{228}Ra between 90 m (the depth of the top of deep waters) and 136 m (the loch floor) during the period between the two cruises can be expressed by the following equations:

$$A_d = A_1 \times 2^{-t/T_{1/2}} \qquad (3)$$

$$I_{ex} = \int_{z_2}^{z_1} (A_2 - A_d) dz \qquad (4)$$

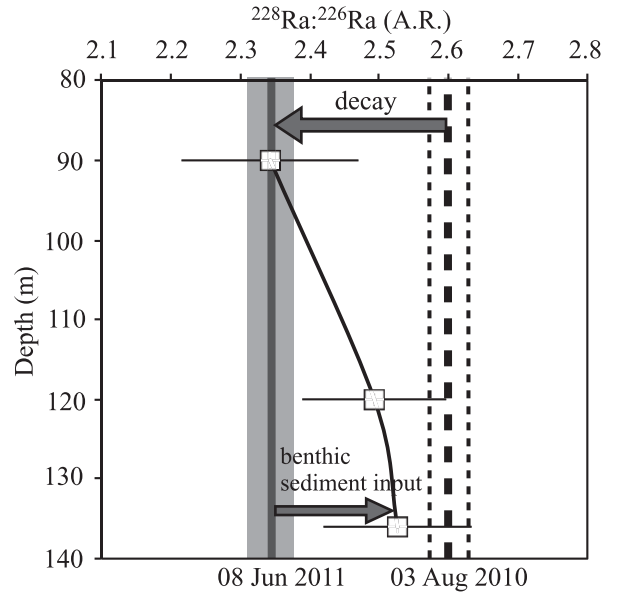of ^{228}Ra (320 mBq 100 L^{-1}) estimated by the radioactive decay; A_1 is the normalized activity of ^{228}Ra (355 mBq

Fig. 9. The activity ratios of ^{228}Ra : ^{226}Ra in the inner deep basin on 08 June 2011. The dashed line is the initial ^{228}Ra : ^{226}Ra on 03 August 2010, calculated as the average of the four deepest samples and shown with 2 SE uncertainty. The gray line is the calculated ^{228}Ra : ^{226}Ra ratio assuming radioactive decay from 03 August 2010 to 08 June 2011. Note that the 90 m sample is well explained by this decay, while deeper samples have a higher ^{228}Ra : ^{226}Ra value, implying addition of ^{228}Ra from sediments on the loch floor.

100 L^{-1}) from the first cruise; A_2 is the normalized activity of ^{228}Ra (320, 340, and 345 mBq 100 L^{-1} at 90 m, 120 m, and 136 m, respectively) from the second cruise; I_{ex} is the depth-averaged integral excess ^{228}Ra inventory: A_2 minus A_d in the water column between z_1 (90 m) and z_2 (136 m) from the second cruise; t is the time between the two cruises (0.85 yr); and $T_{1/2}$ is the half-life of ^{228}Ra (5.75 yr). The integrated excess ^{228}Ra inventory (I_{ex}) is 6900 mBq m^{-2}.

Based on the above equations, the sedimentary ^{228}Ra flux [$F_{sed}(^{228}$Ra)] can be further calculated in the following equation:

$$F_{sed}\left(^{228}\text{Ra}\right) = I_{ex}/t \qquad (5)$$

where $F_{sed}(^{228}$Ra) is the ^{228}Ra sedimentary flux (atoms m^{-2} yr^{-1}). The calculated ^{228}Ra sedimentary flux is 2.1 ± 0.2 ($\times 10^9$) atoms m^{-2} yr^{-1}. This flux is based on the assumption that vertical mixing cannot remove ^{228}Ra from the deep waters, which is justified given the very slow vertical mixing ($K_z \sim 2.5$ cm^2 s^{-1}) in the deep inner loch basin (Inall 2009).

There are several factors controlling the sedimentary Ra flux in estuarine environments: sediment grain size, pore-water diffusive transport (porosity and partition coefficient K_d), bioturbation mixing, sedimentation rate, and Ra production and decay (Cochran and Krishnaswami 1980; Kadko et al. 1987). The new calculated sedimentary flux of 2.1 ± 0.2 ($\times 10^9$) atoms m^{-2} yr^{-1} in the inner basin is ~ 25 times lower than the average global sediment flux of 50 ± 25 ($\times 10^9$) atoms m^{-2} yr^{-1} from the fine-grained shelf

sediments seen in previous studies (Santschi et al. 1979; Cochran 1984; Hancock et al. 2000) but higher than the flux of 1.0 ± 0.5 ($\times 10^9$) atoms m^{-2} yr^{-1} from the coarse-grained shelf sediments (Hancock et al. 2006), as summarized in Moore et al. (2008). Sediments on the continental shelf generally have higher ^{228}Ra flux values, in the range 0.1 to 110 ($\times 10^9$) atoms m^{-2} yr^{-1}, than those on the continental slope, which are in the range 5 to 11 ($\times 10^9$) atoms m^{-2} yr^{-1} (Hammond et al. 1990), or on the deep seafloor, which are in the range 1.4 to 4.3 ($\times 10^9$) atoms m^{-2} yr^{-1} (Cochran and Krishnaswami 1980).

The grain size in the upper 0.60 m of sediment of the Loch Etive inner basin floor has a mean grain size range of 40–70 μm from coarse silt to very fine sand (Howe et al. 2002), which could explain the lower sedimentary ^{228}Ra flux in Loch Etive compared to the average flux from the fine-grained shelf sediments. The sedimentation rate in the inner basin of Loch Etive is relatively high, ~ 0.89 cm yr^{-1} (Ridgway and Price 1987), which may also restrict Ra sediment fluxes. Hancock et al. (2000) suggested that groundwater flow is important to enhance sedimentary Ra fluxes in the estuarine environments, but groundwater flow is insignificant in Loch Etive. The low sedimentary ^{228}Ra flux observed in this study is therefore perhaps not surprising and is consistent with sedimentary fluxes calculated in other settings. It certainly does not indicate an unusually high ^{228}Ra sedimentary flux and therefore supports the assertion that ^{228}Ra inventories in the open ocean require significant input from global groundwater sources (Moore et al. 2008).

The new estimated sedimentary ^{228}Ra flux in Loch Etive improves our understanding of the ^{228}Ra inventory in the ocean, which is important in constraining global freshwater and groundwater discharges to the ocean. Moore et al. (2008) have estimated a substantial discharge of submarine groundwater to the Atlantic, based on the ^{228}Ra inventory in the surface ocean. The estimated total SGD is 2–4 ($\times 10^{16}$) L yr^{-1}, which is about 0.8 to 1.6 times the total river flux to the Atlantic. In their inventory, the referred total sedimentary ^{228}Ra flux (1.3×10^{23} atoms yr^{-1}) is high, about 68% of the total inferred SGD ^{228}Ra flux (1.9×10^{23} atoms yr^{-1}). Assuming that the total sedimentary flux of ^{228}Ra is 25 times lower, based on the new estimate in this study, the inferred SGD ^{228}Ra flux would become 3.2×10^{23} atoms yr^{-1} and the SGD would become 3.4 to 6.7 ($\times 10^{16}$) L yr^{-1}. Thus, SGD may become 1.3 to 2.7 times the river flux to the Atlantic. This rough calculation does not provide any actual estimate of SGD. Nevertheless, it highlights the importance of an improved understanding of sedimentary ^{228}Ra flux to the global freshwater and groundwater discharges in the ocean.

In summary, this study has used a suite of water-column measurements of the Ra quartet to deduce seawater advection rates and sedimentary inputs of Ra in Loch Etive. In the advection-only scenario, the observed decrease of ^{223}Ra with distance from the mouth of the loch at 5 m depth is used to derive a maximum seawater advection rate into the loch of 2.4 ± 0.2 cm s^{-1}. In the mixing-only scenario, the short-lived Ra distribution could be explained by horizontal mixing rates of 6.1×10^6 cm^2 s^{-1} (^{223}Ra$_{ex}$) or 9.1×10^6 cm^2 s^{-1} (^{224}Ra$_{ex}$). Addition of both ^{224}Ra and ^{228}Ra to this subsurface layer is required within the loch. These cannot come only from the river water of River Etive, at the head of the loch, but are instead likely to come largely from shelf sediments of the loch. Sedimentary input of ^{228}Ra is also indicated in deep waters of the inner loch, and a flux of 2.1 ± 0.2 ($\times 10^9$) atoms m^{-2} yr^{-1} is calculated. This value falls at the low end of previous estimate of sedimentary ^{228}Ra fluxes and therefore supports the assertion that open-ocean ^{228}Ra inventories are not explained by sedimentary inputs and require significant input in groundwaters around the globe.

References

Austin, W. E. N., and M. E. Inall. 2002. Deep-water renewal in a Scottish fjord: Temperature, salinity and oxygen isotopes. Polar. Res. **21:** 251–257.

Bollinger, M. S., and W. S. Moore. 1984. Radium fluxes from a salt-marsh. Nature **309:** 444–446.

Broecker, W. S., A. Kaufman, and R. M. Trier. 1973. Residence time of thorium in surface sea-water and its implications regarding rate of reactive pollutants. Earth Planet. Sci. Lett. **20:** 35–44.

———, Y. H. Li, and J. Cromwell. 1967. Radium-226 and radon-222: Concentration in Atlantic and Pacific Oceans. Science **158:** 1307–1310.

Charette, M. A., K. O. Buesseler, and J. E. Andrews. 2001. Utility of radium isotopes for evaluating the input and transport of groundwater-derived nitrogen to a Cape Cod estuary. Limnol. Oceanogr. **46:** 465–470.

Chung, Y. 1980. Radium-barium-silica correlations and a two-dimensional radium model for the world ocean. Earth Planet. Sci. Lett. **49:** 309–318.

Cloern, J. E. 2001. Our evolving conceptual model of the coastal eutrophication problem. Mar. Ecol. Prog. Ser. **210:** 223–253.

Cochran, J. K. 1984. The fates of uranium and thorium decay series nuclides in the estuarine environment, p. 179–220. *In* V. S. Kennedy [ed.], The estuary as a filter. Academic Press.

———, and S. Krishnaswami. 1980. Radium, thorium, uranium, and Pb-210 in deep-sea sediments and sediment pore waters from the north Equatorial Pacific. Am. J. Sci. **280:** 849–889.

Cohen, A. S., and R. K. O'Nions. 1991. Precise determination of femtogram quantities of radium by thermal ionization mass-spectrometry. Anal. Chem. **63:** 2705–2708.

Edwards, A., and D. J. Edelsten. 1977. Deep water renewal of Loch Etive-3 Basin Scottish Fjord. Estuar. Coast. Mar. Sci. **5:** 575–595.

———, and B. E. Grantham. 1986. Inorganic nutrient regeneration in Loch Etive bottom water. The role of freshwater outflow in coastal marine ecosystem. Springer-Verlag, NATO ASI Series **G7:** 195–204.

———, and F. Sharples. 1986. Scottish sea lochs: A catalogue. Scottish Marine Biological Association Special Publication.

Foster, D. A., M. Staubwasser, and G. M. Henderson. 2004. ^{226}Ra and Ba concentrations in the Ross Sea measured with multicollector ICP mass spectrometry. Mar. Chem. **87:** 59–71.

Geibert, W., M. Charette, G. Kim, W. S. Moore, J. Street, M. Young, and A. Paytan. 2008. The release of dissolved actinium to the ocean: A global comparison of different end-members. Mar. Chem. **109:** 409–420.

Hammond, D. E., R. A. Marton, W. M. Berelson, and T. L. Ku. 1990. ^{228}Ra distribution and mixing in San-Nicolas and San-Pedro basins, southern California borderland. J. Geophys. Res. Oceans **95:** 3321–3335.

Hancock, G. J., I. T. Webster, P. W. Ford, and W. S. Moore. 2000. Using Ra isotopes to examine transport processes controlling benthic fluxes into a shallow estuarine lagoon. Geochim. Cosmochim. Acta **64:** 3685–3699.

———, ———, and T. C. Stieglitz. 2006. Horizontal mixing of Great Barrier Reef waters: Offshore diffusivity determined from radium isotope distribution. J. Geophys. Res. Oceans **111:** C12019, doi:10.1029/2006JC003608

Howe, J. A., W. E. N. Austin, M. Forwick, M. Paetzel, R. Harland, and A. G. Cage. 2010. Fjordic systems and archives: A review. Geological Society, London, Special Publications **344:** 5–15.

———, J. Overnell, M. E. Inall, and A. D. Wilby. 2001. A side-scan sonar image of a glacially-overdeepened sea loch, upper Loch Etive, Argyll. Scot. J. Geol. **37:** 3–10.

———, T. Shimmield, W. E. N. Austin, and O. Longva. 2002. Post-glacial depositional environments in a mid-high latitude glacially-overdeepened sea loch, inner Loch Etive, western Scotland. Mar. Geol. **185:** 417–433.

Hsieh, Y. T., and G. M. Henderson. 2011. Precise measurement of ^{228}Ra/^{226}Ra ratios and Ra concentrations in seawater samples by multi-collector ICP mass spectrometry. J. Anal. Atom. Spectrom. **26:** 1338–1346.

Inall, M. E. 2009. Internal wave induced dispersion and mixing on a sloping boundary. Geophys. Res. Lett **36:** L05604, doi:10.1029/2008GL036849

———, F. Cottier, C. Griffiths, and T. Rippeth. 2004. Sill dynamics and energy transformation in a jet fjord. Ocean Dynam. **54:** 307–314.

Kadko, D., J. K. Cochran, and M. Lyle. 1987. The effect of bioturbation and adsorption gradients on solid and dissolved radium profiles in sediments from the eastern equatorial Pacific. Geochim. Cosmochim. Acta **51:** 1613–1623.

Karakassis, I., M. Tsapakis, E. Hatziyanni, K. N. Papadopoulou, and W. Plaiti. 2000. Impact of cage farming of fish on the seabed in three Mediterranean coastal areas. ICES J. Mar. Sci. **57:** 1462–1471.

Kaufman, A., R. M. Trier, W. S. Broecker, and H. W. Feely. 1973. Distribution of ^{228}Ra in world ocean. J. Geophys. Res. **78:** 8827–8848.

Ku, T. L., and S. D. Luo. 1994. New Appraisal of ^{226}Ra as a large-scale oceanic mixing tracer. J. Geophys. Res. Oceans **99:** 10255–10273.

———, and ———. 2008. Ocean circulation mixing studies with decay-series isotopes, p. 307–344. *In* S. Krishnaswami and J. K. Cochran [eds.], U-series nuclides in aquatic systems. Elsevier.

Li, Y. H., and L. H. Chan. 1979. Desorption of Ba and ^{226}Ra from river-borne sediments in the Hudson estuary. Earth Planet. Sci. Lett. **43:** 343–350.

Moore, W. S. 1998. Application of ^{226}Ra, ^{228}Ra, ^{223}Ra, and ^{224}Ra in coastal waters to assessing coastal mixing rates and groundwater discharge to oceans. Proc. Indian Acad. Sci. Earth Planet. Sci. **107:** 343–349.

———. 2000*a*. Determining coastal mixing rates using radium isotopes. Cont. Shelf Res. **20:** 1993–2007.

———. 2000*b*. Ages of continental shelf waters determined from ^{223}Ra and ^{224}Ra. J. Geophys. Res. **105:** 22117–22122.

———. 2008. Fifteen years experience in measuring ^{224}Ra and ^{223}Ra by delayed-coincidence counting. Mar. Chem. **109:** 188–197.

———, and R. Arnold. 1996. Measurement of ^{223}Ra and ^{224}Ra in coastal waters using a delayed coincidence counter. J. Geophys. Res. Oceans **101:** 1321–1329.

———, R. M. Key, and J. L. Sarmiento. 1985. Techniques for precise mapping of Ra-226 and Ra-228 in the Ocean. J. Geophys. Res. Oceans **90:** 6983–6994.

———, J. L. Sarmiento, and R. M. Key. 2008. Submarine groundwater discharge revealed by ^{228}Ra distribution in the upper Atlantic Ocean. Nat. Geosci. **1:** 309–311.

Overnell, J., T. Brand, W. Bourgeois, and P. J. Statham. 2002. Manganese dynamics in the water column of the upper basin of Loch Etive, a Scottish fjord. Estuar. Coast. Shelf Sci. **55:** 481–492.

Porcelli, D., and P. W. Swarzenski. 2003. The behavior of U- and Th-series nuclides in groundwater. Rev. Mineral. Geochem. **52:** 317–361.

Rama, and W. S. Moore. 1996. Using the radium quartet for evaluating groundwater input and water exchange in salt marshes. Geochim. Cosmochim. Acta **60:** 4645–4652.

Ridgway, I. M., and N. B. Price. 1987. Geochemical associations and postdepositional mobility of heavy-metals in coastal sediments—Loch-Etive, Scotland. Mar. Chem. **21:** 229–248.

Rutgers van der Loeff, M. M., R. M. Key, J. Scholten, D. Bauch, and A. Michel. 1995. ^{228}Ra as a tracer for shelf water in the Arctic Ocean. Deep-Sea Res. II **42:** 1533–1553.

Santschi, P. H., Y.-H. Li, J. J. Bell, and R. M. Trier. 1979. Natural radionuclides in the water of Narragansett Bay. Earth Planet. Sci. Lett. **51:** 248–265.

Sarmiento, J. L., H. W. Feely, W. S. Moore, A. E. Bainbridge, and W. S. Broecker. 1976. Relationship between vertical eddy diffusion and buoyancy gradient in deep-sea. Earth Planet. Sci. Lett. **32:** 357–370.

Scholten, J. C., K. P. Mai, O. Blinova, M. A. Charette, H. Dulaiova, and M. Eriksson. 2010. Preparation of Mn-fiber standards for the efficiency calibration of the delayed coincidence counting system (RaDeCC). Mar. Chem. **121:** 206–214.

Skogen, M. D., M. Eknes, L. C. Asplin, and A. D. Sandvik. 2009. Modeling the environmental effects of fish farming in a Norwegian fjord. Aquaculture **298:** 70–75.

Stahl, H. [ed.]. 2011. Set-up and implementation of in situ observatories for monitoring oxygen depletion and associated parameters in land-locked water bodies (Swiss Lakes, Koljö Fjord, Loch Etive, Ionian Sea lagoon) and data collection into the HYPOX web portal. EU seventh framework programme report deliverable 7.1. Online at http://www.hypox.net/upload/deliverables/D7-1_V3_110609.pdf

STASHCHUK, N., M. INALL, AND V. VLASENKO. 2007. Analysis of supercritical stratified tidal flow in a Scottish Fjord. J. Phys. Oceanogr. **37:** 1793–1810.

STATHAM, P. J., AND OTHERS. 2005. Spatially complex distribution of dissolved manganese in a fjord as revealed by high-resolution in situ sensing using the autonomous underwater vehicle autosub. Environ. Sci. Technol. **39:** 9440–9445.

STRANEO, F., R. G. CURRY, D. A. SUTHERLAND, G. S. HAMILTON, C. CENEDESE, K. VAGE, AND L. A. STEARNS. 2011. Impact of fjord dynamics and glacial runoff on the circulation near Helheim Glacier. Nat. Geosci. **4:** 322–327.

TAMMEMAGI, H. Y. 1976. Radioelement concentrations in British Tertiary Granites. Geol. Mag. **113:** 271–276.

VAN BEEK, P., M. BOURQUIN, J. L. REYSS, M. SOUHAUT, M. A. CHARETTE, AND C. JEANDEL. 2008. Radium isotopes to investigate the water mass pathways on the Kerguelen Plateau (Southern Ocean). Deep-Sea Res. II **55:** 622–637.

WEBSTER, I. T., G. J. HANCOCK, AND A. S. MURRAY. 1994. Use of radium isotopes to examine pore-water exchange in an estuary. Limnol. Oceanogr. **39:** 1917–1927.

WOOD, B. J. B., P. B. TETT, AND A. EDWARDS. 1973. Introduction to phytoplankton, primary production and relevant hydrography of Loch Etive. J. Ecol. **61:** 569–585.